# Supplementary Information

# Single emission spectrum measurement enables control of organic LED emission zone giving ultralong device lifetime

**R. Mac Ciarnáin[1,2*], H.W. Mo[3], K. Nagayoshi[3], H. Fujimoto[3,4], K. Harada[3,4], R. Gehlhaar[1], T. H. Ke[1], P. Heremans[1,2] & C. Adachi[3,4]**

*rmacc@t-online.de
[1]IMEC Kapeldreef 75, 3001, Leuven, Belgium
[2]KU Leuven, Oude Markt 13, 3000 Leuven, Belgium
[3]i[3]-opera, 5-14 Kyudai-shimmachi, Nishi, Fukuoka, 819-0388, Japan
[4]OPERA, Kyushu University, 744 Motooka, Nishi, Fukuoka 819-0395, Japan.

# Contents

## S1 Additional improvements to the conventional angular, destructive interference microcavity emission zone measurement method

Possible reasons for a Gaussian solution not being reported in the literature are now outlined:

(a) Fitting to an error below the experimental error.
This can be avoided by stopping the fitting when the fitting error is equal to the experimental error [1]. See methods section also.

(b) Simultaneously fitting the EZ and the internal spectrum.
The simulation in Fig.5 of this work used a fixed molecular spectrum. In [2], the molecular spectrum was varied at the same time as the EZ in the fitting, simultaneously fitting two unknown parameters in one linear equation. The resulting spectrum was named “PL spectrum” [2] but a comparison with a real photoluminescence spectrum was not shown. An extreme example of this fitting process is shown in Supplementary Fig. 20 to show the possibility of errors. If s-polarization and p-polarization experimental data are interchanged, the EZ and molecular spectrum in the simulation can compensate for the wrong experimental data and fit it well. The extracted molecular spectrum then fits the PL spectrum badly (in this work the molecular spectra, shown in Fig.5b, all follow the PL shape closely, allowing for shifts in wavelength due to concentration quenching. Even when the correct experimental data is used, the EZ and molecular spectrum could change together in a circular logic to give false results. The molecular spectrum can, as in this work, be extracted independently from *bright* devices (Supplementary Fig. 3) where the effect of the EZ on the emission spectrum is low (Fig. 1a).

(c) The importance of the microcavity thickness accuracy.
The position accuracy of the extracted EZ is directly dependent on the accuracy of the device emitter ensemble - cathode distance and so stack thickness errors should be carefully addressed. If the 155 nm EML + ETL thickness in [2] would have a 10% error, which is plausible for thermally evaporated doped multilayers [3,4,5], then the resulting emission zone positional accuracy could be around half the EML thickness (similarly to the example shown in Supplementary Fig. 19). However, these previous publications [2,6] do not give a microcavity thickness error estimation or discussion. Transient electroluminescence turn-off peaks (also measured for the stacks of this work in Supplementary Fig. 13) presented as evidence of the U-shaped emission zones in [2,6], could also be explained by carriers trapped at the blocking layer interfaces existing alongside a Gaussian emission zone. The single shot method outlined in this work can be easily used to re-test these U-shaped EZ results with a more sensitive method.

It should also be noted that a sensing layer study by the same group as [6] on a similar OLED except using B3PYMPM instead of B4PYMPM as electron transporter and an additional 8% concentration of $Ir(ppy)_2acac$ emitter had a result of a constant EZ across the EML [7].

## S2 Further discussion of degradation mechanisms

With a higher emitter concentration, more energy processes occur on the more stable 4CzIPN emitter than the mCBP host [8], which should also increase the device stability. The larger EZ shift for emitter concentrations of 20% and 30% in Fig.5d, should be because the charge balance at 20% and 30% is closer to a less stable equilibrium, further from the interfaces, where a small decrease in hole transport allows the electron transport to dominate and shift the charge balance. Conversely, with the 10% device, even if the hole transport decreases, the EZ is still fixed at the HBL interface, due to the relative lack of electron carriers. There should also be less electron injection too from a degraded HBL, but the EZ changes observed suggest that host degradation dominates. This is surprising, by only observing the red peak, and not using the single shot EZ measurement, one would expect the EZ shift to occur in the opposite direction.

The EZ peaks for 10, 20 and 30% emitter concentration with the Bpy-TP2 ETL, in Fig.5d are not exactly at the EML-HBL interface possibly due to higher interface quenching with this HBL and ETL combination, see Supplementary Fig. 11.

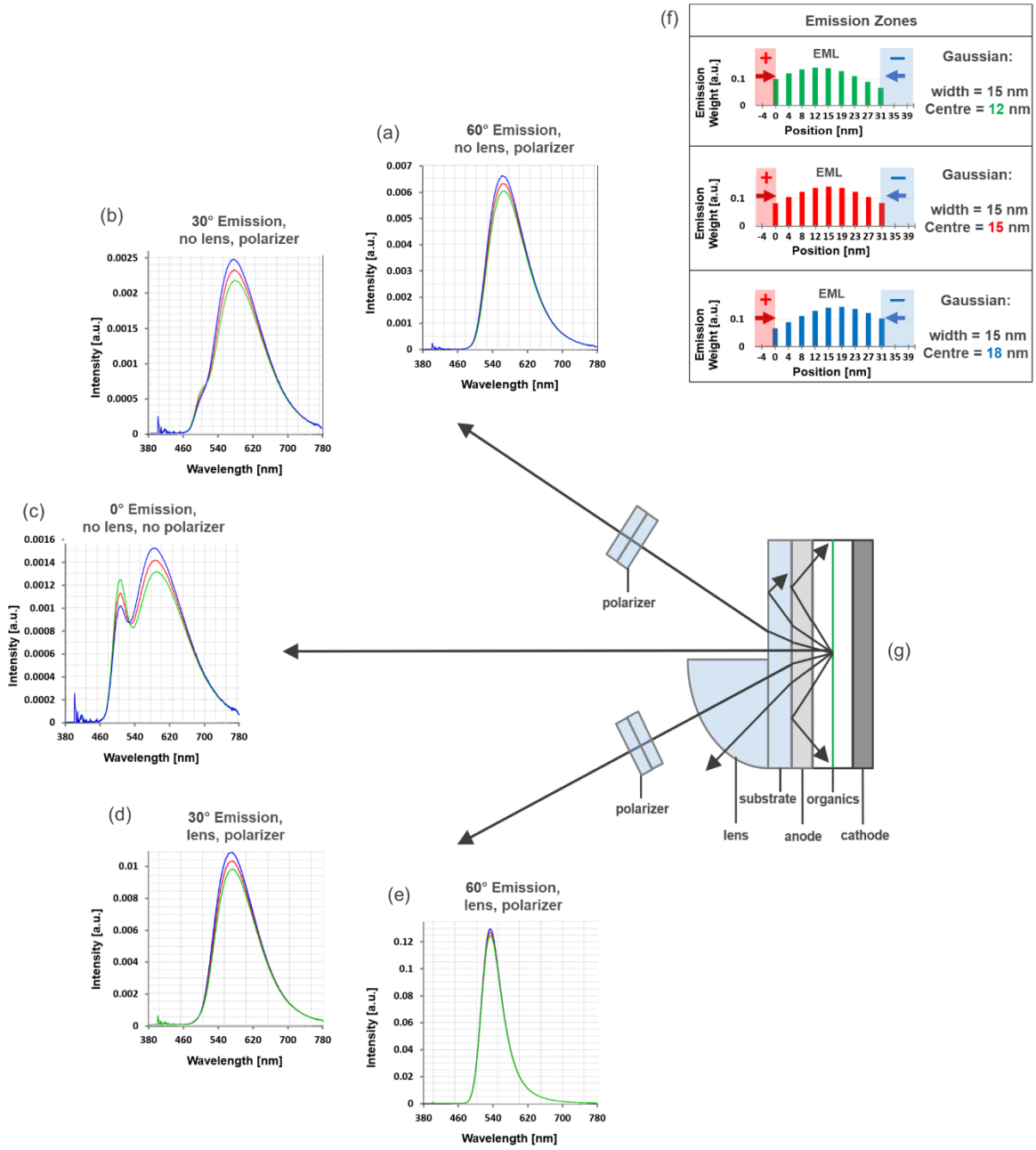


**Fig. S1** Three emission zones (EZs), shifted by 3 nm in position in the emission layer (EML), along the layer normal of the OLED are shown in part (f). These slightly different EZs are used to check the sensitivity of the optical measurement to EZ changes. All EZs have a Gaussian width of 15 nm, however, the top one, in green, is centred 3 nm to the anode side, the middle one, in red, is centred in the centre of the EML. The lower one is centred 3 nm to the cathode side, shown in blue. Simulated spectra for these three emission zones are shown for different measurement conditions (a-e). Each emission zone's colour is also shown as the resulting emission spectrum colour. Polarizers need to be used at angles other than layer-normal (0°) emission (the direction perpendicular to the OLED layers) to separate emitter orientation effects from emission zone effects [9]. A cylindrical lens is placed on the OLED, seen in the lower half of (g), as used in [2,6]. In the simulation, the emitter ensemble – cathode distance is set to give the destructive interference resonance most visible for normal (0°) emission (the direction perpendicular to the OLED layers). This simulation uses a 100 nm BPy-TP2 ETL. It can be seen that, for 0° emission, the destructive interference resonance is

positioned clearly on the emission spectrum, and the spectrum sensitivity to emission zone is high. One can observe, that measurement data from higher angles using a more complicated angular measurement setup do not have a good emission zone sensitivity. One cannot easily distinguish the emission spectra from the three EZs at higher angles. Therefore the highest emission zone sensitivity is obtained by measuring a single angle where the destructive interference resonance is well positioned on the emission spectrum by choosing a correct emitter-cathode thickness. Lower sensitivity would result from also using the lower sensitivity data from the higher angles in a fitting procedure.

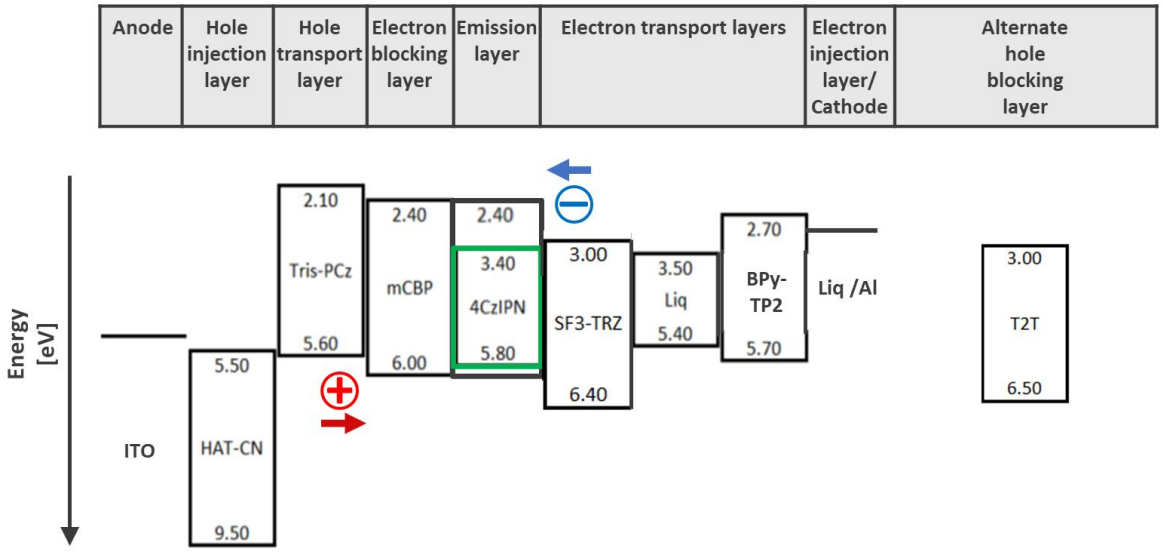


**Fig. S2** Charge transport energy levels. The lowest unoccupied molecular orbital (LUMO) energy levels, where electrons can hop, are shown above in the graph and the highest occupied molecular orbital (HOMO) energy levels, where holes can hop, are shown below. These are equivalent to conduction band and valence band respectively in inorganic semiconductors. Injection energy levels from the ITO anode and the Liq /Al cathode are also sketched. Electrons should favourably inject into the EML on the 4CzIPN emitter and not on the mCBP host. If the emitter concentration is low, then there could be an electron accumulation at the EML – HBL interface. The “electron blocking layer” in this stack actually acts more as a buffer layer as Tris-PCz can quench excitons formed in the emission layer.

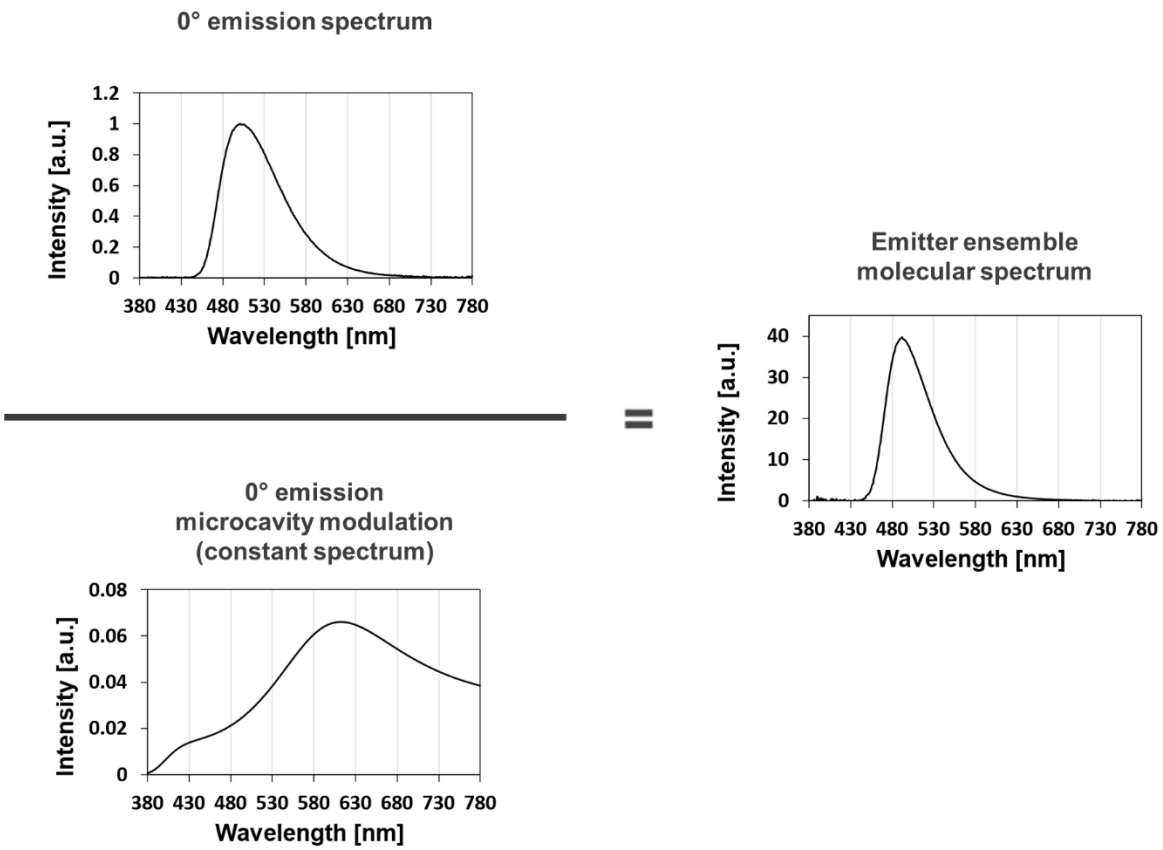


**Fig. S3** The equation used for the extraction of the emitter ensemble molecular spectrum from *bright* devices to get the molecular spectrum independently from the emission zone fitting procedure. The EZ has only a small effect on the emission spectrum of *bright* devices (Fig.1). The 0° emission spectrum is experimentally measured and the 0° emission microcavity modulation for constant spectrum (value of 1 for all wavelengths) is simulated using the n&k and thickness values of the device layers. The 0° emission direction is shown in Fig.1. Then, the only unknown in the equation is the emitter ensemble molecular spectrum.

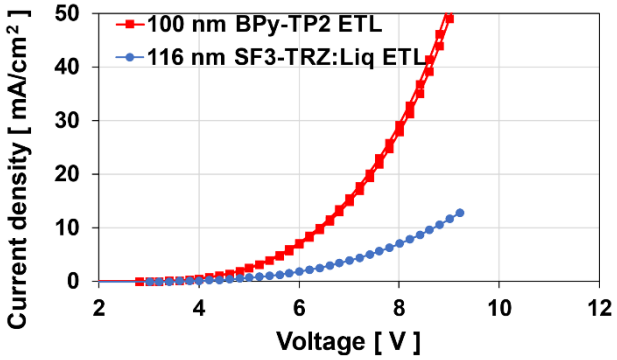


**Fig. S4** Current density-voltage curves for the 100 nm Bpy-TP2 ETL device and the 116 nm SF3-TRZ:Liq ETL device, both with HTL = 30 nm and 30% emitter concentration.

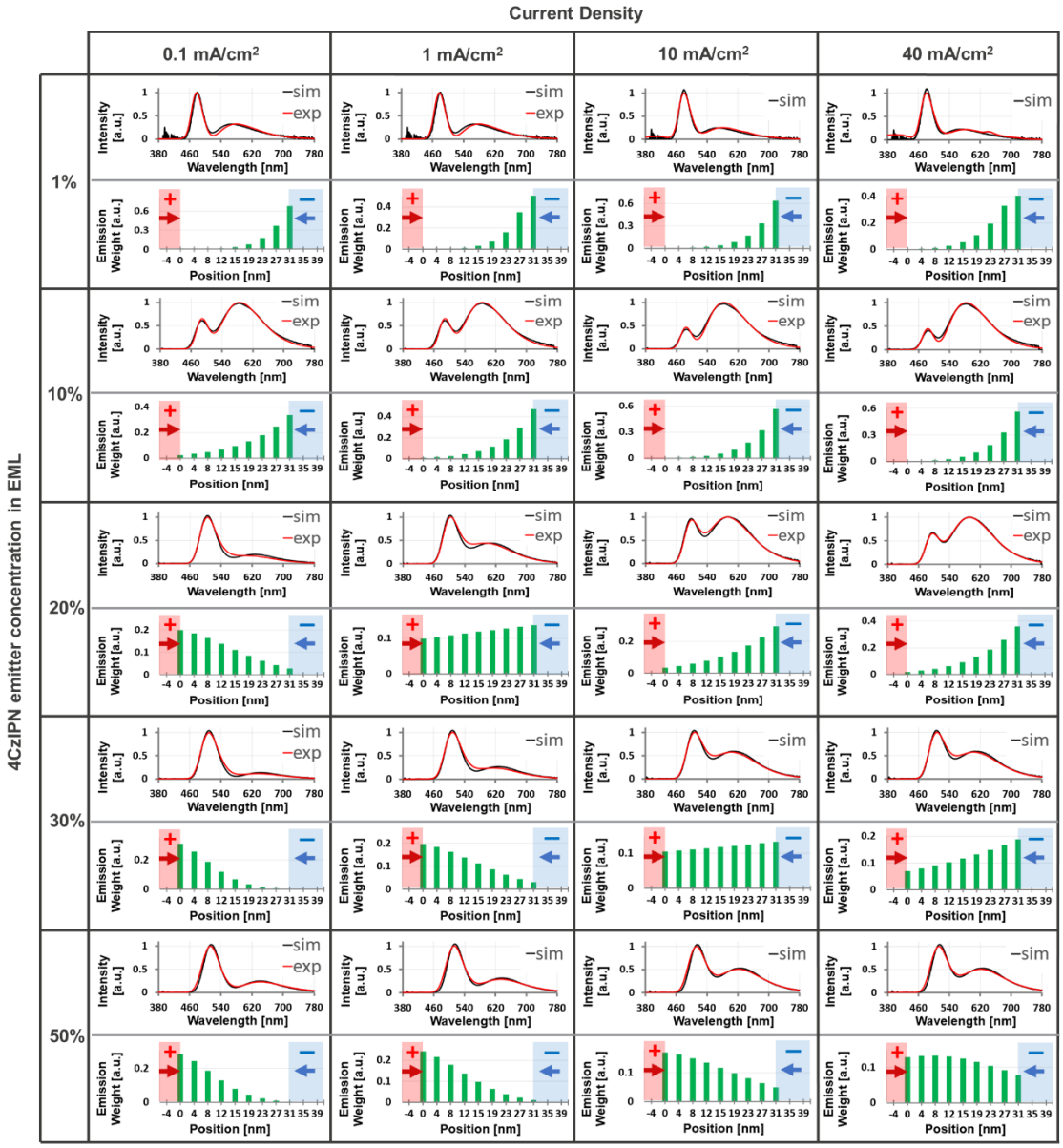


**Fig. S5** Spectral fitting and resulting emission zone profiles for *dark* SF3-TRZ:Liq devices. Above graphs of each table entry show measured (red) and simulated (black) 0° emission spectra. Simulated curves are noisy due to using an experimentally extracted molecule spectrum. Below graphs show the EZ as weighted emission source positions in EML (green bars) which give the simulated spectrum above. The simulated spectra are fitted to the experimental while varying only the EZ as a discretized Gaussian function. These are the only EZ solutions found. Each row represents a single device. The top three rows are from a single deposition with ETL = 116 nm where only the emitter concentration of each substrate quarter is varied by use of a shutter. The bottom three rows are from another deposition of ETL thickness not more than 1 nm different (see methods section for thickness accuracy details). Changes in a row of spectra are caused only by a varying EZ with current density. Spectral changes along columns are due to the EZ changing with emitter concentration and to a lesser degree, concentration-quenching shifted [10] molecular spectra (Fig.5b), which are independently extracted from *bright* devices (Supplementary Fig. 3) and input into each simulation. The small differences compared to Fig. 3 can be explained by the experimental error in the EZ centre position (as in Supplementary Fig.19), except for perhaps at 40 mA/cm2, which is discussed in Supplementary discussion S2.

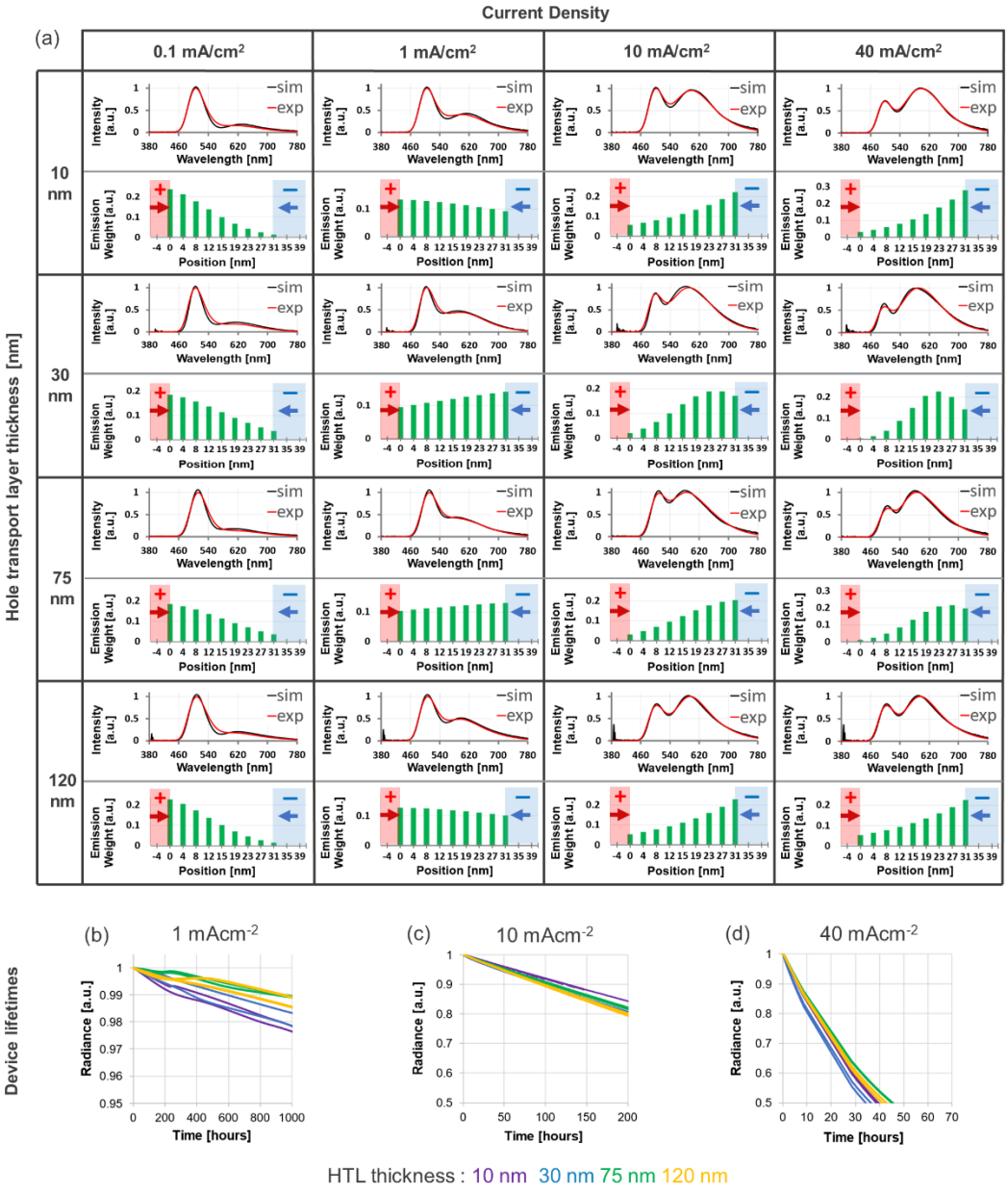


**Fig. S6** Emission zone (a) and lifetime comparison at different current densities (b,c,d) for HTL thickness variation and 20% emitter concentration with the *dark* BPy-TP2 ETL. EZs and lifetimes are not notably different for the different HTL thickness devices.

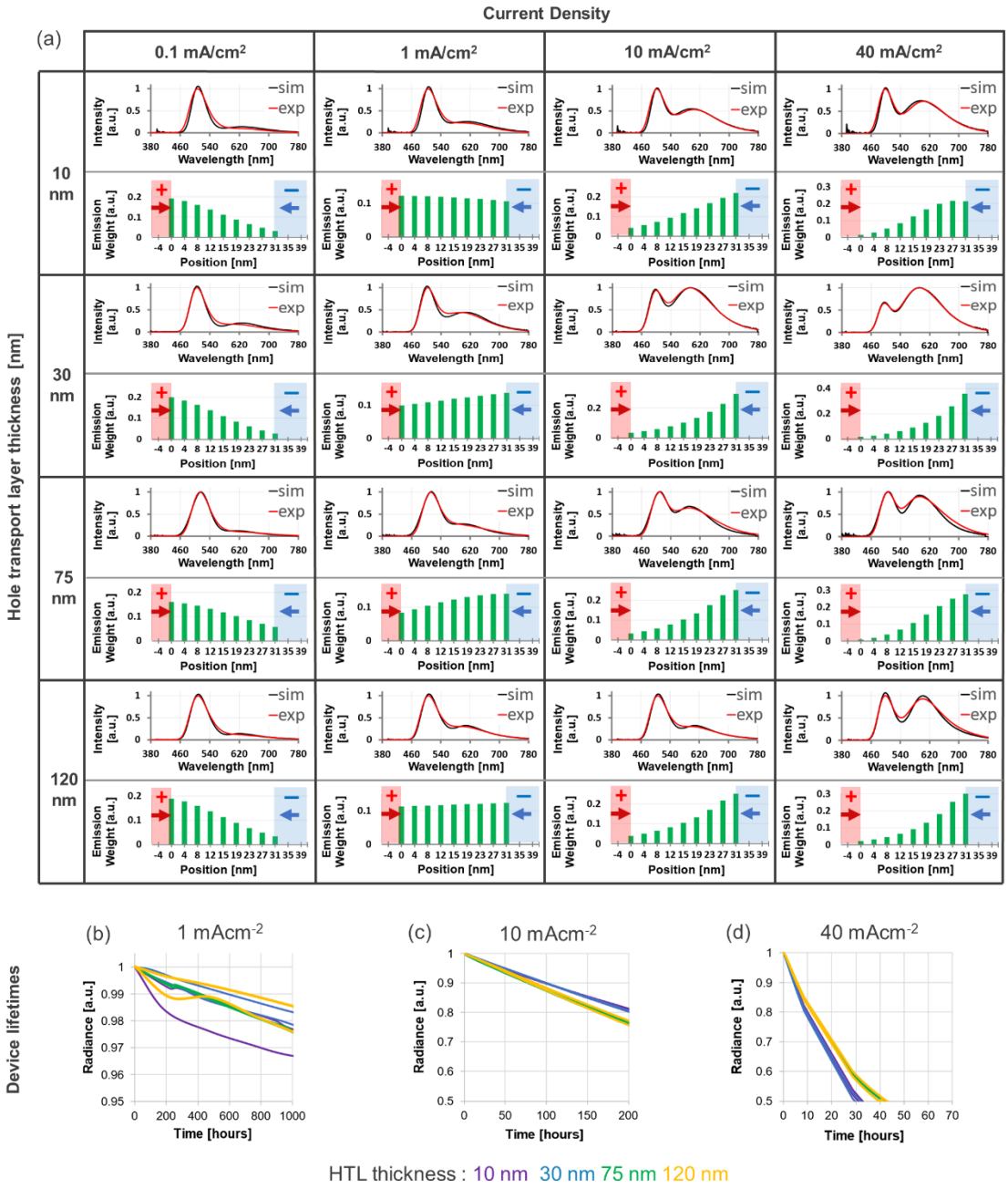


**Fig. S7** Emission zone (a) and lifetime comparison at different current densities (b,c,d) for HTL thickness variation and 20% emitter concentration with the *dark* SF3-TRZ:Liq ETL. EZs and lifetimes are not notably different for the different HTL thickness devices.

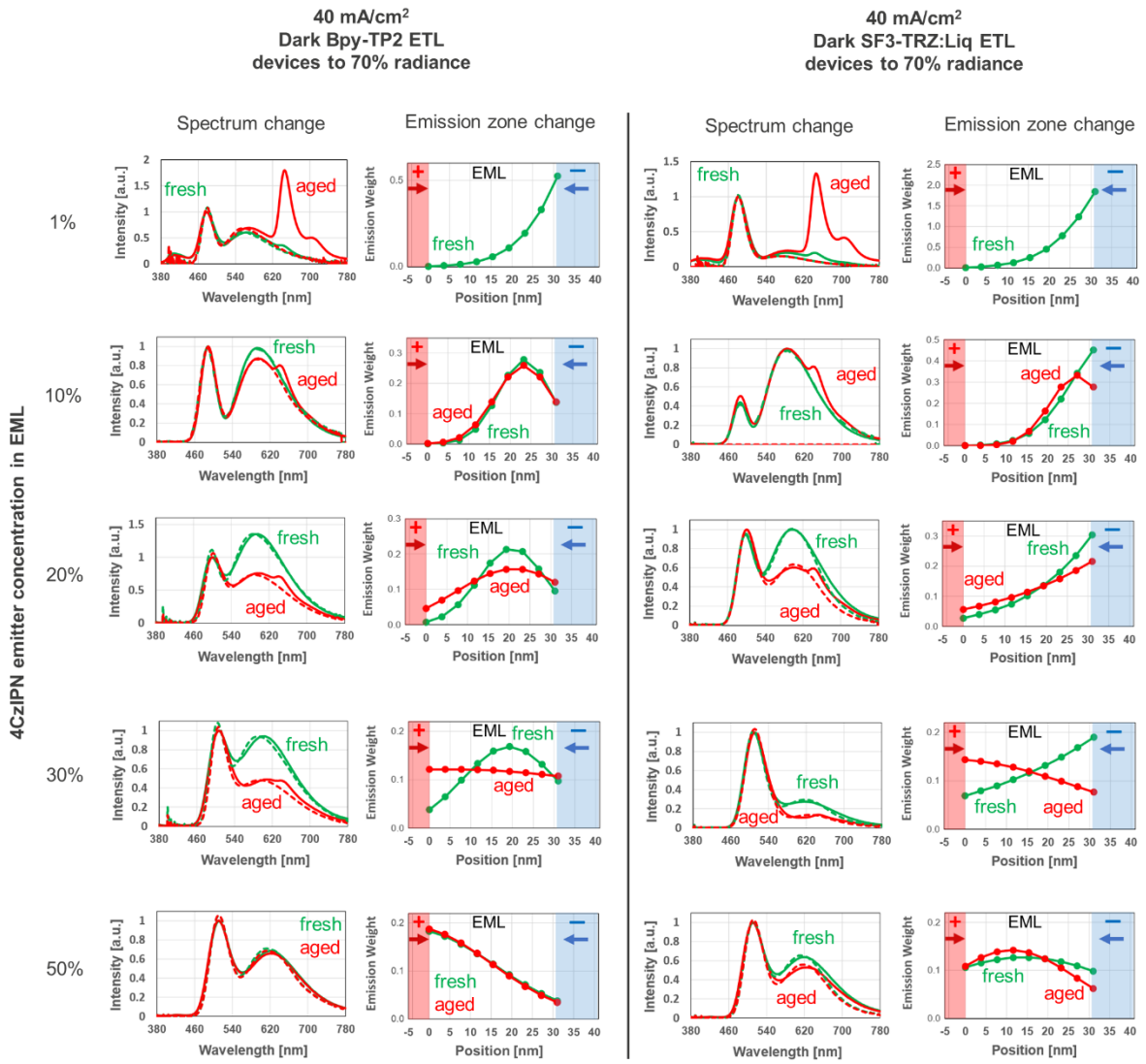


**Fig. S8** Spectral and emission zone changes with 40 mA/cm2 driving to 50% radiance for the two different ETLs. Fresh (green lines) and aged (red lines) spectra are shown on the left sides, experimental curves are denoted by solid lines and simulated curves dashed. Corresponding EZs which fit the fresh and aged spectra are shown on the right. Dots on the curves show the (Gaussian) discrete emission weights of the simulation. Peaks at 640 nm are emission from the HBL [11] Aged emission zones cannot be calculated for the 1% devices as the level of HBL emission is too high. These spectra are slightly different than in Fig.3 because different devices in the same deposition run, characterised to have slightly different thicknesses must be used for different lifetime measurements.

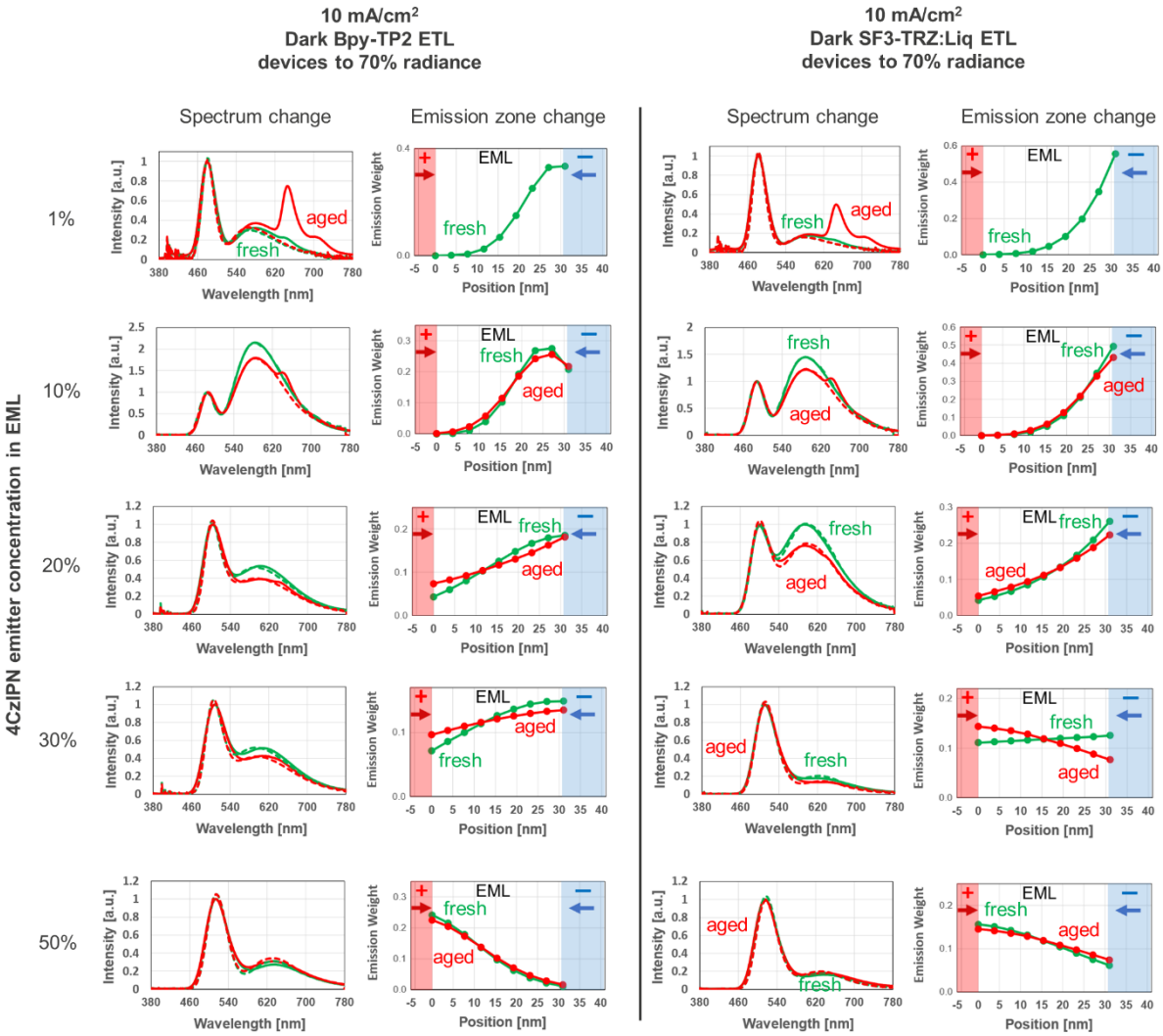


**Fig. S9** Spectral and emission zone changes with 10 mA/cm2 driving to 70% radiance for the two different ETLs. Fresh (green lines) and aged to 50% radiance (red lines) spectra are shown on the left sides, experimental curves are denoted by solid lines and simulated curves dashed. Corresponding EZs which fit the fresh and aged spectra are shown on the right. Dots on the curves show the (Gaussian) discrete emission weights of the simulation. Peaks at 640 nm are emission from the HBL [11] Aged emission zones cannot be calculated for the 1% devices as the level of HBL emission is too high. These spectra are slightly different than in Fig.3 because different devices in the same deposition run, characterised to have slightly different thicknesses must be used for different lifetime measurements.

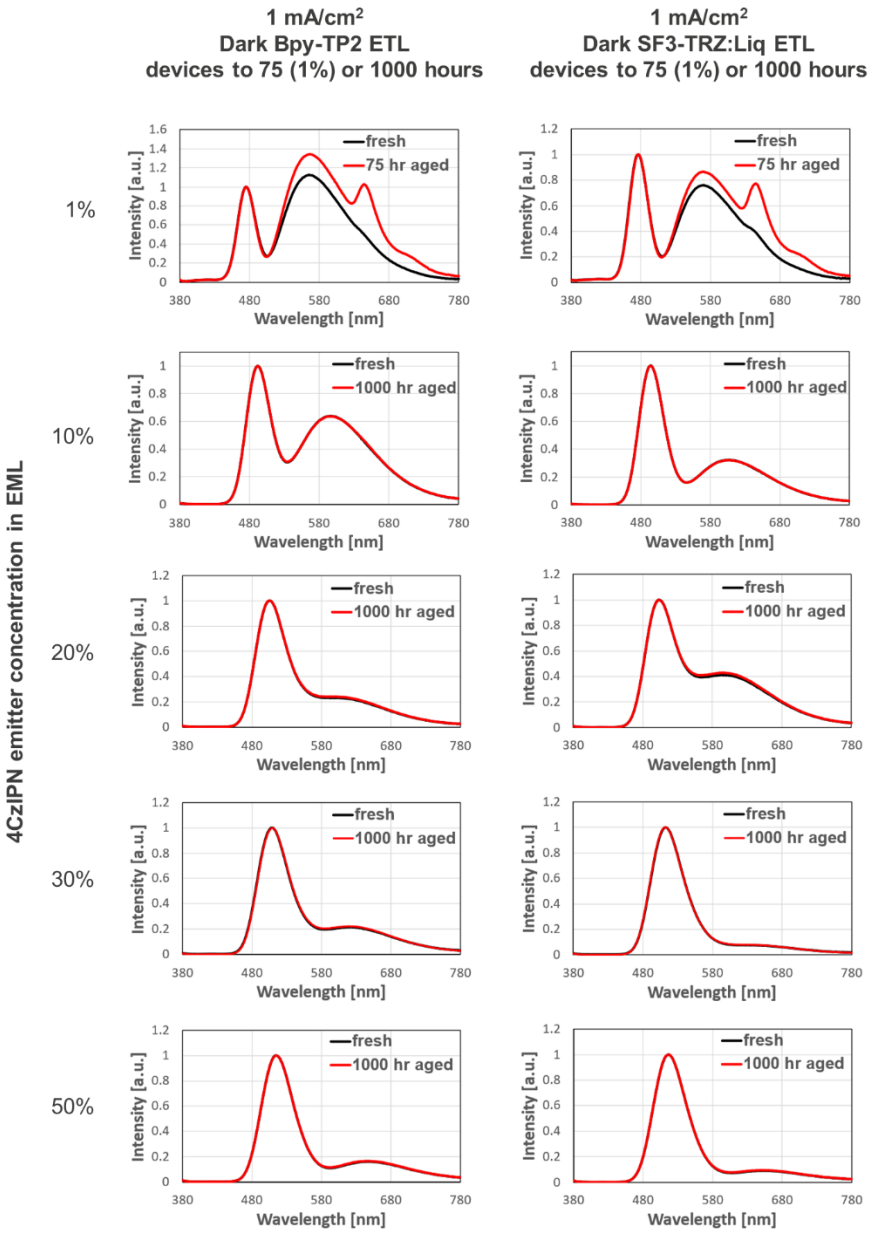


**Fig. S10** Spectral changes at 1 mA/cm$^2$ current density after 75 (1%) or 1000 hours driving for both *dark* ETLs. The 1% devices stopped measuring after 75 hours as the radiance reached the chosen limit level of 50%. Fresh spectra are shown with black lines and aged with red lines. HBL emission is only visible for the 1% devices where the EZ is very concentrated at the HBL interface. No significant spectral changes which would indicate EZ changes or HBL emission are visible for emitter concentrations higher than 1%. It seems that not many holes enter the HBL of the non-1% devices at this current density.

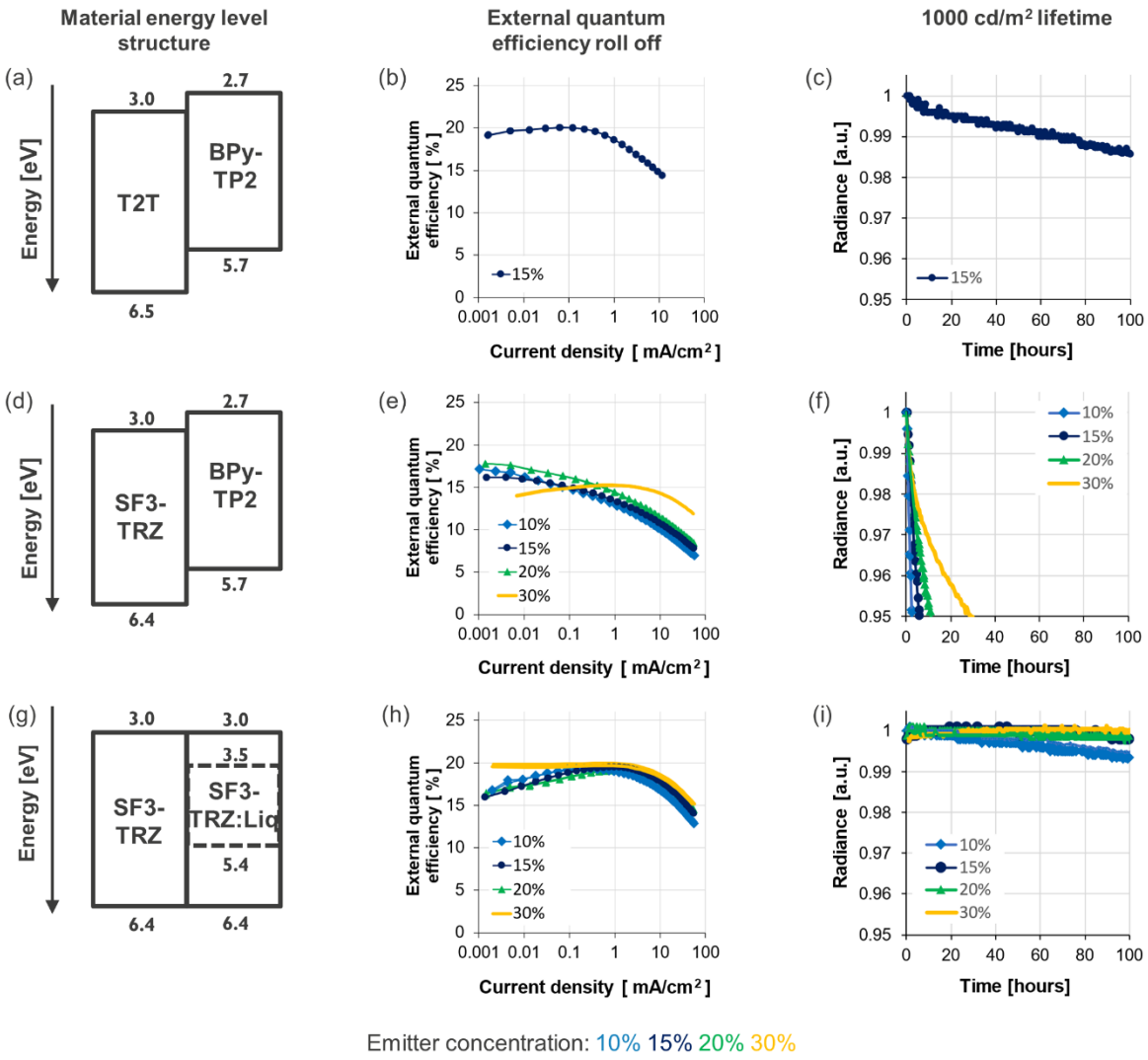


**Fig. S11** Charge transport energy levels (a,d,g), EQE roll off (b,e,h) and lifetime at 1000 cd/m$^2$ (c,f,i) are shown for different HBL and thin ETL (34 nm for BPy-TP2, otherwise 40 nm) combinations. The best choice ETL for a low driving voltage was BPy-TP2 but a very short lifetime resulted at 1000 cd/m$^2$ (f). The degraded spectra were analysed and 640 nm HBL emission occurred strongly for the BPy-TP2 ETL device, but not the SF3-TRZ:Liq ETL device (Supplementary Fig. 12). The thin BPy-TP2 ETL device should have comparable EZs as the dark ETL devices as it has the same HBL emission trend with EZ in Supplementary Fig. 12. A much higher EQE roll-off, even at lower current densities resulted with structure (d) devices of less than 30% emitter concentration, but not for the other two structures (a,g). At the higher 30% concentration, where the EZ is away from EML-HBL interface, the issue is lessened. Unlike with structure (g), with the structure (d), a large spectral blue shift and so a shift of the emission zone to the HBL side (principal shown in [11]) was observed (Supplementary Fig. 12), indicating that the electron transport in the EML degraded more than the hole transport. Therefore, a different degradation process than for the other structures should dominate. Additionally, more charge detrapping was measured for the thin BPy-TP2 ETL structure (d) devices (Supplementary Fig. 13). Such a short device lifetime did not occur (c), when the HBL was replaced with T2T (structure (a)), which has the same HOMO level and a close LUMO level to SF3-TRZ (Supplementary Fig. 2). The T2T HBL device also requires a lower driving voltage. It could be that some interface charge effect occurs with the combination of SF3-TRZ and 34 nm thick Bpy-TP2 ETL, resulting in a fast ageing of the device. This effect is not significant with a 100 nm thick BPy-TP2 ETL, possibly due to a reduced capacitance. Perhaps holes can cross to the HBL-ETL interface to the

convenient HOMO level of BPy-TP2 and recombine with accumulated electrons there causing the large HBL emission/degradation and a decreasing electron transport in the EML. This phenomenon should be further studied using electrical methods.

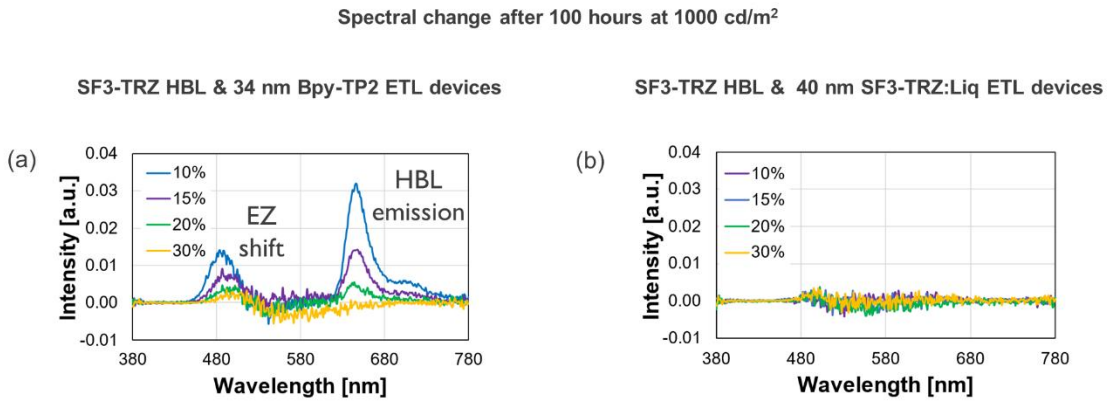


**Fig. S12** Emission spectra changes with 100 hour 1000 cd/m$^2$ device driving time for devices of various emitter concentration with different ETLs. The shown spectral data are aged spectra subtracted from fresh. Around 500 nm, spectral change due to an EZ shift [11] can be observed and around 640 nm, HBL emission [11].

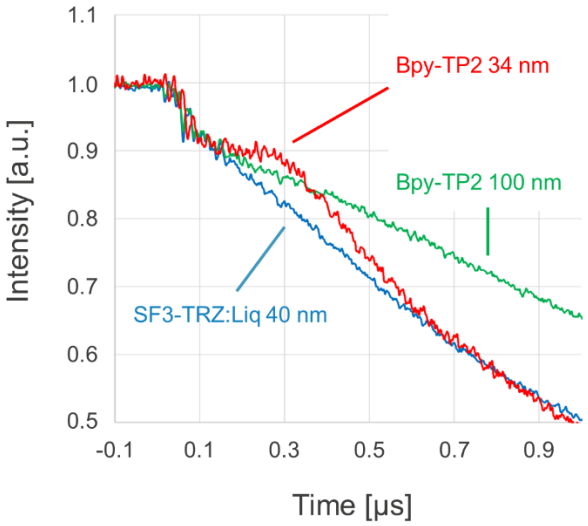


**Fig. S13** Charge detrapping for different ETLs. A voltage of +10 V is applied to excite the OLED, then at time = 0 the pulse is set to -10 V to pull charges out of traps in the opposite direction to recombine and emit light. More charge detrapping is observed for the thinner than the thicker BPy-TP2 ETL device. Detrapping is not observed for the 40 nm SF3-TRZ:Liq ETL device.

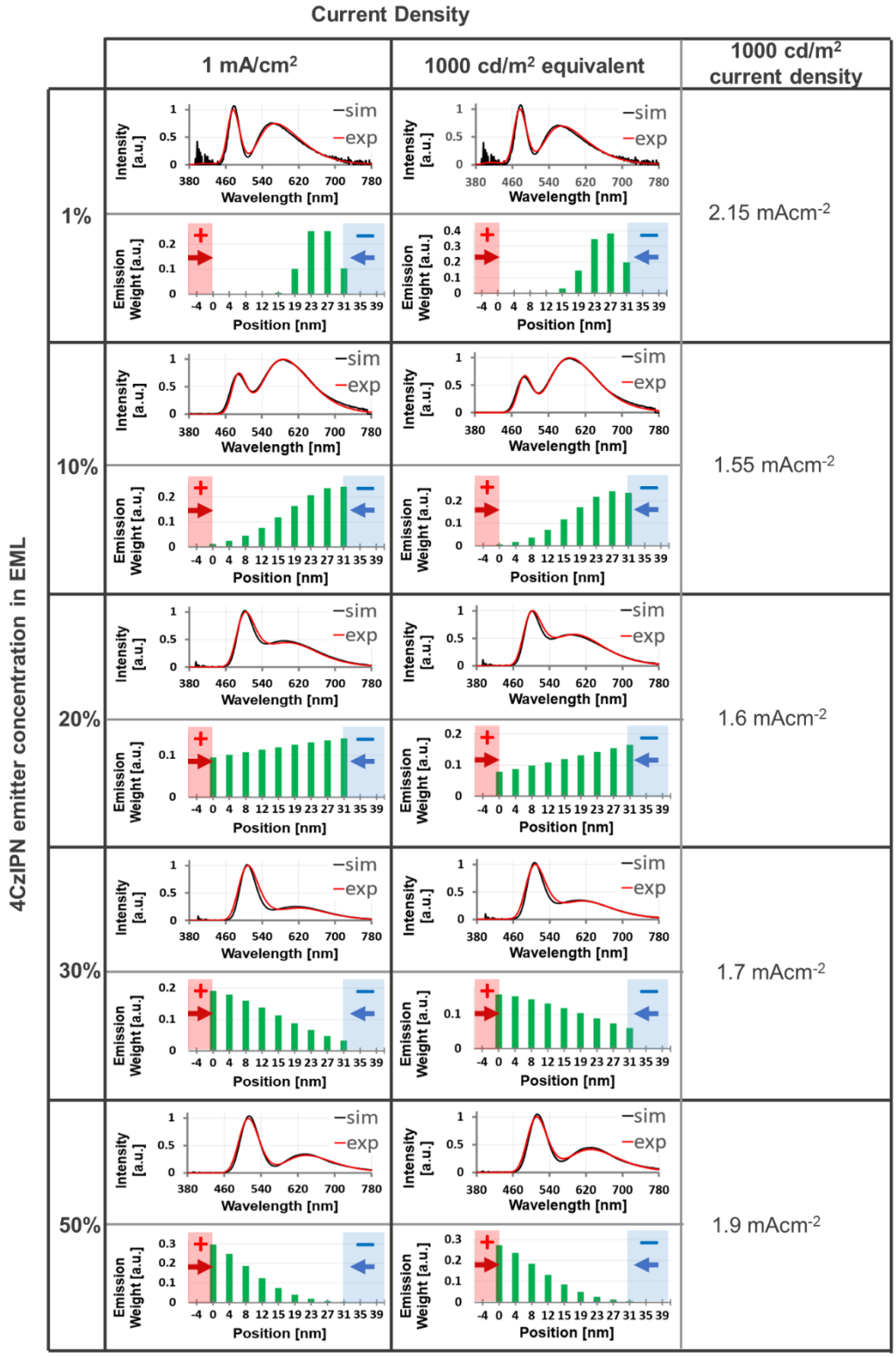


**Fig. S14** *Dark* device EZs at 1 mA/cm$^2$ (left side) compared with the *dark* device EZs at the same current densities as the *bright* devices need to give 1000 cd/m$^2$ (right side). We assume that the *bright* and *dark* device EZs are comparable, as discussed in the main paper. Different emitter concentration devices require different current densities to give 1000 cd/m$^2$.

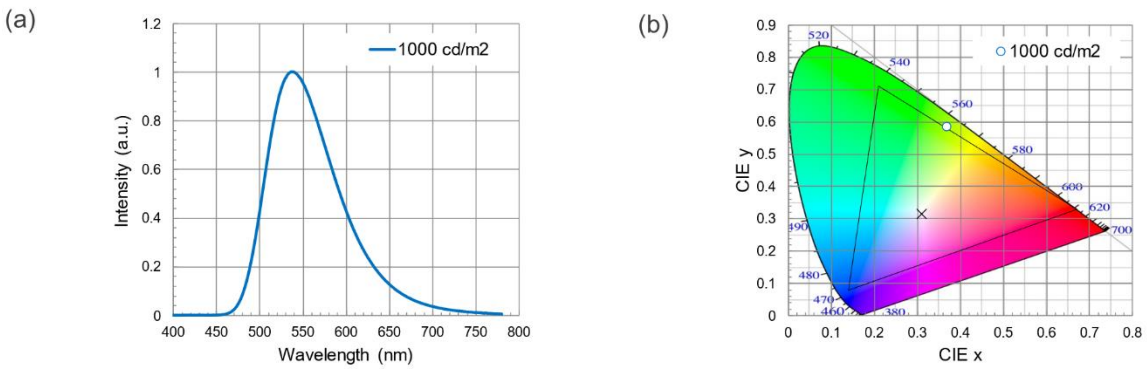


**Fig. S15** (a) 1000 cd/m$^2$ electroluminescence emission spectrum measured at normal direction to the layer planes, i.e., 0° emission and (b) 1000 cd/m$^2$ CIE colour coordinates of the 30% device with a 30 nm HTL and a 40 nm SF3-TRZ:Liq ETL. This device gives an EQE of 20% and measured T95 lifetime at 1000 cd/m$^2$ of 4500 hours.

| Emitter concentration | Photoluminescence quantum yield (PLQY) |
|---|---|
| 1% | 95.2 +/- 1.0 % |
| 10% | 81.9 +/- 0.8 % |
| 15% | 79.0 +/- 0.8 % |
| 18% | 77.3 +/- 0.8 % |
| 25% | 77.2 +/- 0.8 % |
| 30% | 77.2 +/- 0.8 % |
| 40% | 72.0 +/- 0.7 % |
| 62.5% | 59.5 +/- 0.6 % |
| 75% | 52.1 +/- 0.5 % |
| 87.5% | 44.6 +/- 0.4 % |
| 100% | 35.8 +/- 0.4 % |

**Fig. S16** PLQY for different 4CzIPN concentrations in mCBP, measured from a deposited 50 nm thick film. The shown measurement error was estimated as 1% of the measured value.

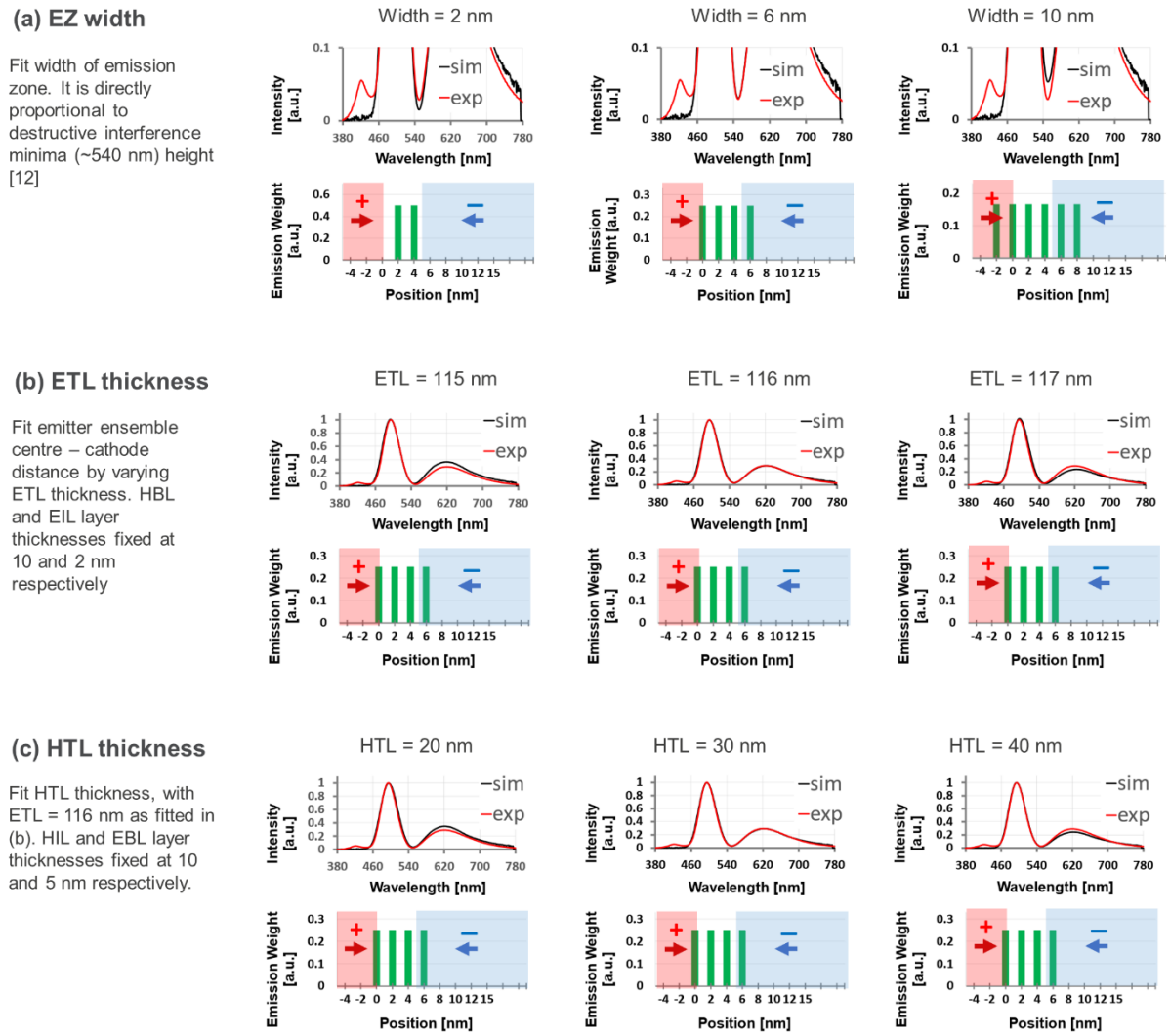


**Fig. S17** Steps for high accuracy thickness fitting of actual deposited microcavity, without requiring ellipsometry. Fitting of an emission spectrum measurement results in higher accuracy than ellipsometry as it is an actual measurement of the real device and not a separate sample and also offers better than 1 nm thickness accuracy of ellipsometry. Fitting for a 6 nm EML device is shown as a good example of the method's sensitivity. The measurement current density here is 10 mA/cm$^2$. (a) the emission zone width is varied so that the destructive interference minimum of the simulated spectrum fits the experimentally measured spectrum. Measured additional blue emission is most likely from the mCBP EML host [8,11]. (b) The ETL thickness is varied in the simulation so that the destructive interference minimum shifts to the same place as in the experimentally measured spectrum. (c) The HTL thickness has a lesser microcavity effect, due to the lesser reflectivity of the ITO anode resulting in less reflection and so interference on this side. This results in a similar spectral change being caused by a 10 nm difference rather than a 1 nm difference in the ETL variation case.

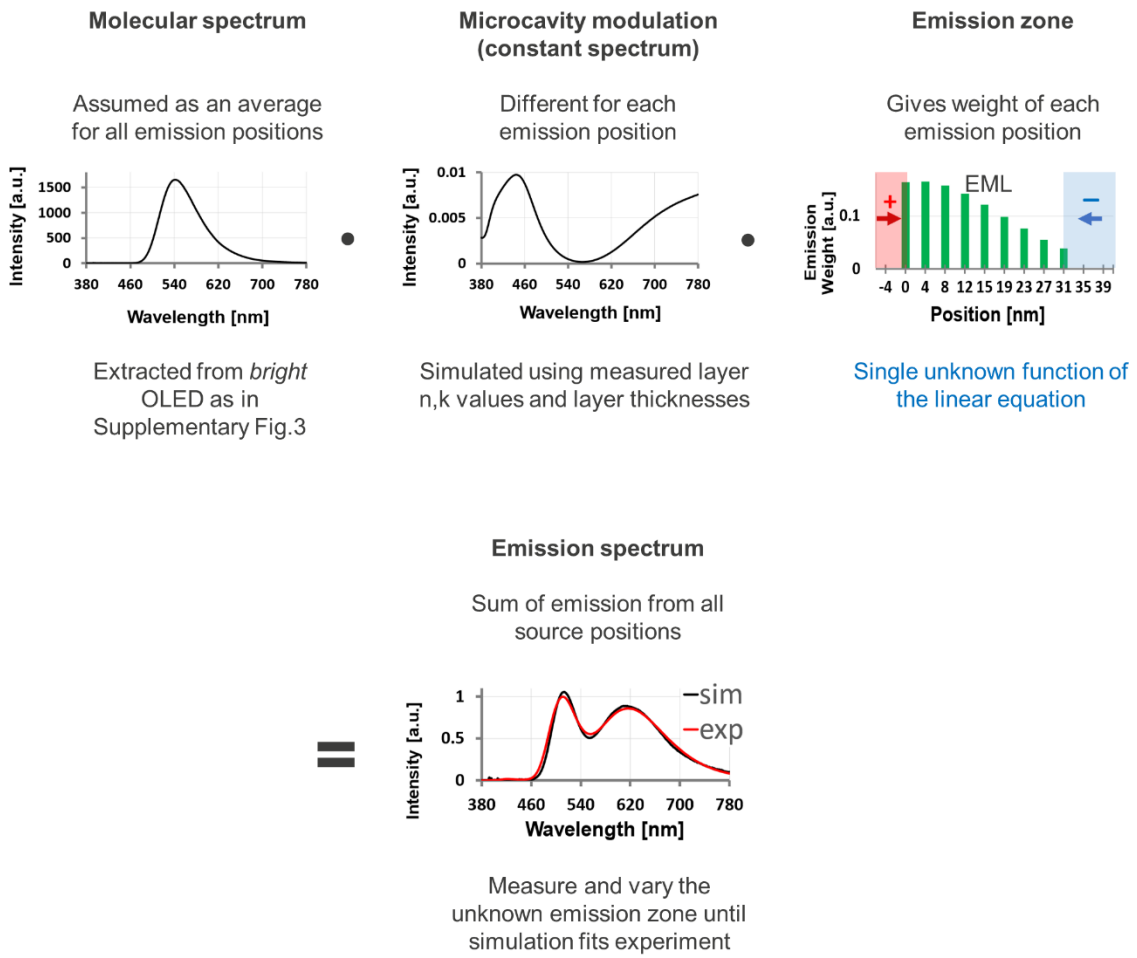


**Fig. S18** A schematic of the OLED emission linear equation. When extracting the molecular spectrum from a different *bright* OLED, the only unknown to vary to fit to the experimental spectrum is the emission zone. For emission measured normal to the OLED layers (0°), emitter orientation effects can be neglected [9]. Further theoretical details of the linear equation are given in [13].

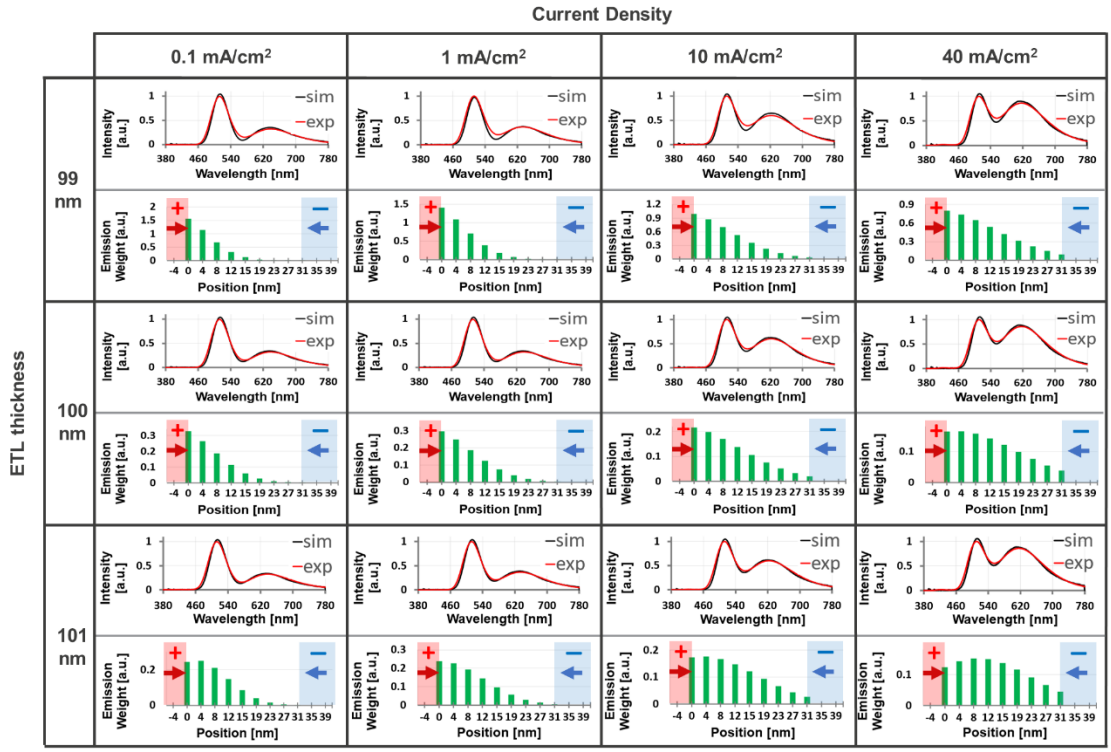


**Fig. S19** Error range in emission zone centre position resulting from a 1 nm uncertainty in ETL thickness, for a 50% emitter concentration Bpy-TP2 ETL device. If, in the simulation, the emitter-cathode distance is incorrect, then the centre of the emission zone will shift position to compensate, so that the emitter-cathode distance is correct to fit the experimental spectrum, resulting in an error in the actual emission zone centre position. One can observe the resulting emission zone shift from the left to the right from the 99 nm ETL case to the 101 nm ETL case.

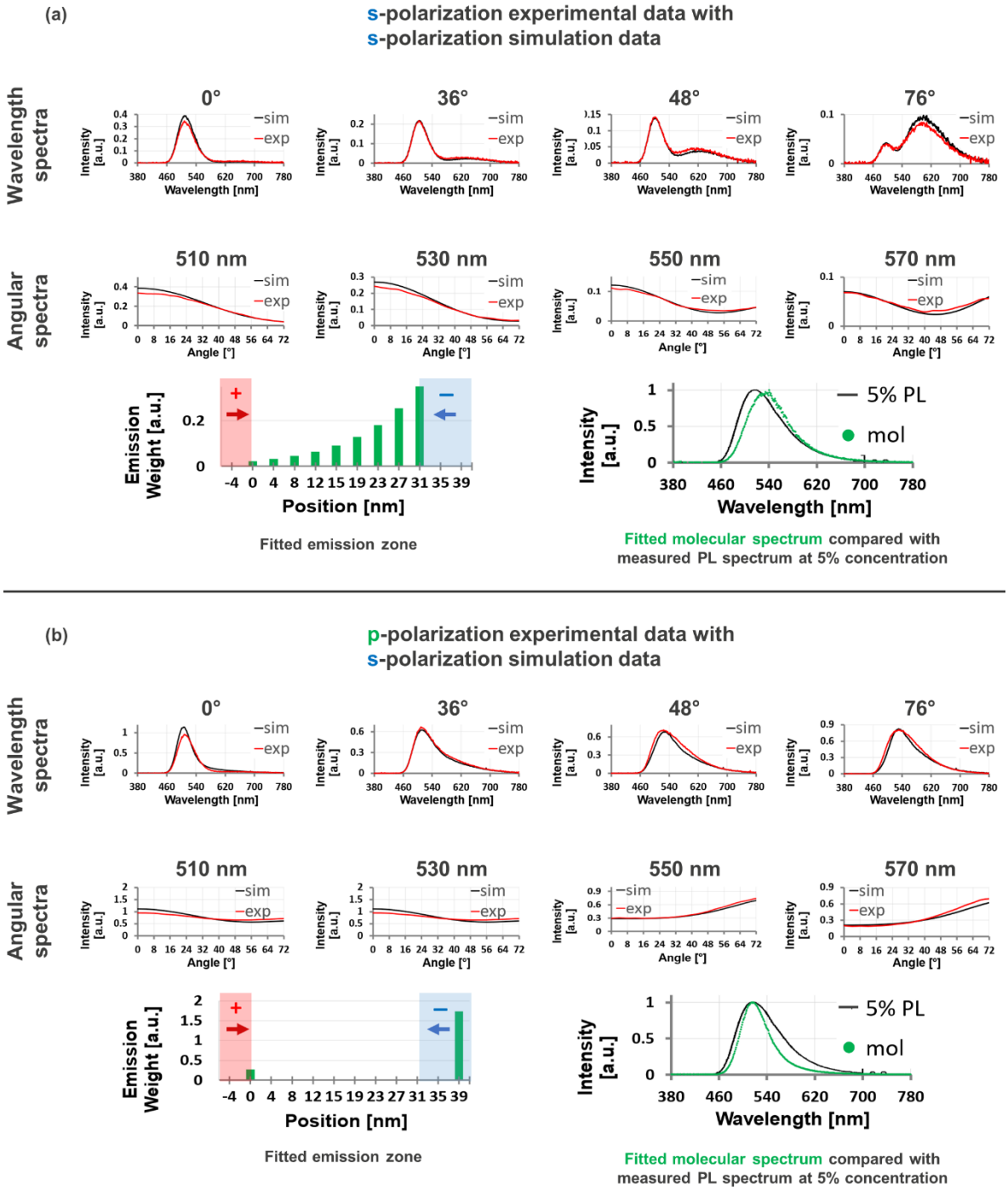


**Fig. S20** Varying the emission zone profile and molecular spectrum at the same time when fitting s-polarization experimental spectra and s-polarization simulation (a) and with p-polarization experimental spectra and s-polarization simulation (b). This is an extreme example which shows how errors can occur when varying two parameters (the molecular spectrum and the emission zone) simultaneously to fit a single linear equation (equation diagrammatically sketched in Supplementary Fig. 18). The measurements and simulation are for a 20% emitter concentration device with a thicker 125 nm SF3-Liq ETL. The red shift of the extracted molecular spectrum in (a) is expected (see Fig. 5b) as the emitter concentration of the device measured is 20% compared with 5% for the PL measurement. However, the thinning of the spectrum in part (b) cannot be explained and should be due to an artifact error due to varying two parameters simultaneously while fitting a single linear equation. It also does not match the extracted molecular spectra in Fig. 5b. The PL measurement is from [14].

## S3 References


[1] Mac Ciarnain, R. et al. Emission from outside of the emission layer in state-of-the-art phosphorescent organic light-emitting diodes. *Organic Electronics* **44,** 115-119 (2017).

[2] Regnat, M. et al. Analysis of the bias-dependent split emission zone in phosphorescent OLEDs. *ACS Appl. Mater. Interfaces* **10**, 31552−31559 (2018).

[3] Celii, F.G., Harton, T.B. & Phillips, O.F. Characterization of organic thin films for OLEDs using spectroscopic ellipsometry. *Journal of electronic materials* **26.4,** 366-371 (1997).

[4] Nabatova-Gabain, N., Wasai, Y. & Tsuboi, T. Spectroscopic ellipsometry study of $Ir(ppy)_3$ organic light emitting diode. *Current Applied Physics* **6(5),** 833-838. (2006).

[5] Fujimoto, H. et al. Novel methodology for reproducibility of OLED lifetimes and identification of killer impurities. *SID Symposium Digest of Technical Papers* **51-1,** 822-825 (2020).

[6] Regnat, M. et al. Routes for efficiency enhancement in fluorescent TADF exciplex host OLEDs gained from an electro-optical device model. *Adv. Electron. Mater.* **6,** 1900804 (2020).

[7] Sim, B., Moon, C.-K., Kim, K.-H. & J.-J. Kim. Quantitative analysis of the efficiency of OLEDs. *ACS Appl. Mater. Interfaces **8***, 33010 (2016).

[8] Wang, P. et al. The electroluminescence mechanism of solution-processed TADF emitter 4CzIPN doped OLEDs investigated by transient measurements. *Molecules* **21,** 1365 (2016).

[9] Mac Ciarnain, R. et al. Plasmonic Purcell effect reveals obliquely ordered phosphorescent emitters in Organic LEDs. Scientific Reports 7, 1826 (2017).

[10] Kim, H.S., Park, S.R., & Suh, M.C. Concentration quenching behavior of thermally activated delayed fluorescence in a solid film. *J. Phys. Chem. C* **121**, 13986−13997 (2017).

[11] Tanaka, M., Noda, H., Nakanotani, H., & Adachi, C. Effect of carrier balance on device degradation of organic light-emitting diodes based on thermally activated delayed fluorescence emitters. *Adv. Electron. Mater.* **5,** 1800708 (2019).

[12] Epstein, A., Roberts, M, Tessler, N, & Einziger P.D. Analytical estimation of emission zone mean position and width in organic light-emitting diodes from emission pattern image-source interference fringes. *Journal of Applied Physics **115,** 223101 (2014).*

[13] Danz, N. et al. OLED Emission Zone measurement with high accuracy. *Organic Light Emitting Materials and Devices XVII, Proc. of SPIE* **8829**, 882923 (2013).

[14] Niwa et al. Temperature dependence of photoluminescence properties in a thermally activated delayed fluorescence emitter. *Appl. Phys. Lett.* **104**, 213303 (2014).